Check for updates

New Phytologist

Research

An AP2/ERF transcription factor ERF139 coordinates xylem cell expansion and secondary cell wall deposition

Bernard Wessels[1]*, Carolin Seyfferth[1]*, Sacha Escamez[1], Thomas Vain[2], Kamil Antos[3], Jorma Vahala[4], Nicolas Delhomme[2], Jaakko Kangasjärvi[4], Michaela Eder[5], Judith Felten[2] and Hannele Tuominen[1]

[1]Department of Plant Physiology, Umeå Plant Science Centre, Umeå University, Umeå SE-90187, Sweden; [2]Department of Forest Genetics and Plant Physiology, Umeå Plant Science Centre, Swedish University of Agricultural Sciences, Umeå SE-90183, Sweden; [3]Department of Integrative Medical Biology, Umeå University, Umeå SE-90187, Sweden; [4]Organismal and Evolutionary Biology Research Programme, Faculty of Biological and Environmental Sciences, Viikki Plant Science Centre, VIPS, University of Helsinki, Viikinkaari 1 (POB65), Helsinki FI-00014, Finland; [5]Department of Biomaterials, Max Planck Institute of Colloids and Interfaces, Potsdam 14476, Germany

Author for correspondence:
Hannele Tuominen
Tel.: +46 90 786 9693
Email: Hannele.tuominen@umu.se

Received: *3 March 2019*
Accepted: *19 May 2019*

New Phytologist (2019) **224:** 1585–1599
doi: 10.1111/nph.15960

Key words: cell expansion, ethylene response factor (ERF), hybrid aspen, lignin, *Populus*, secondary growth, xylem development.

Summary

- Differentiation of xylem elements involves cell expansion, secondary cell wall (SCW) deposition and programmed cell death. Transitions between these phases require strict spatiotemporal control.
- The function of *Populus ERF139* (*Potri.013G101100*) in xylem differentiation was characterized in transgenic overexpression and dominant repressor lines of *ERF139* in hybrid aspen (*Populus tremula* × *tremuloides*). Xylem properties, SCW chemistry and downstream targets were analyzed in both types of transgenic trees using microscopy techniques, Fourier transform-infrared spectroscopy, pyrolysis-GC/MS, wet chemistry methods and RNA sequencing.
- Opposite phenotypes were observed in the secondary xylem vessel sizes and SCW chemistry in the two different types of transgenic trees, supporting the function of ERF139 in suppressing the radial expansion of vessel elements and stimulating accumulation of guaiacyl-type lignin and possibly also xylan. Comparative transcriptomics identified genes related to SCW biosynthesis (LAC5, LBD15, MYB86) and salt and drought stress-responsive genes (ANAC002, ABA1) as potential direct targets of ERF139.
- The phenotypes of the transgenic trees and the stem expression profiles of *ERF139* potential target genes support the role of ERF139 as a transcriptional regulator of xylem cell expansion and SCW formation, possibly in response to osmotic changes of the cells.

Introduction

Wood, or secondary xylem, formation is a developmental program which begins with cell division in the vascular cambium, followed by expansion, secondary cell wall (SCW) deposition and ultimately programmed cell death of the cambial derivatives (Lucas *et al.*, 2013; Smet & De Rybel, 2016). The SCWs consist of three major polymers – cellulose, hemicelluloses and lignin – which together maintain the overall structure and strength of the plant (Gorshkova *et al.*, 2015). SCW biosynthesis is orchestrated by evolutionarily conserved transcriptional mechanisms. The Arabidopsis NAC domain transcription factors (TFs) VASCULAR-RELATED NAC-DOMAIN6 (VND6) and VND7 regulate xylem vessel differentiation, while NAC SECONDARY WALL THICKENING PROMOTING FACTOR1 (NST1) and SECONDARY WALL-ASSOCIATED NAC DOMAIN PROTEIN1 (SND1) have been described as regulators of the transcriptional network underlying SCW deposition in fibers (for a recent review, see Ohtani *et al.*, 2017). The direct targets of the NAC domain TFs include SCW biosynthetic, cell wall-modifying, and cell death genes, as well as TFs such as MYBs (Chen *et al.*, 2019). Less is known about the upstream regulators of these key TFs, even though gene regulatory network analyses suggested that the cell cycle regulator E2Fc is a putative direct regulator of vessel differentiation through VND6 and 7 (Taylor-Teeples *et al.*, 2015), whereas LOB DOMAIN-CONTAINING PROTEIN15 (LBD15) was identified as a positive regulator of VND7 (Ohashi-Ito *et al.*, 2018).

The APETALA2/ethylene response factors (AP2/ERFs) are TFs that have been frequently implicated in regulation of xylem differentiation and wood formation but that are functionally poorly described (Seyfferth *et al.*, 2018). Evidence is accumulating, however, that AP2/ERF TFs may play a role in lignin biosynthesis (Ambavaram *et al.*, 2011; Vahala *et al.*, 2013; Taylor-Teeples *et al.*, 2015; Lee *et al.*, 2016). Heterologous overexpression of the Arabidopsis AP2/ERF *SHINE* in rice resulted in a 45% reduction in lignin content compared with the wild-type (WT) (Ambavaram *et al.*, 2011). Another AP2/ERF stimulated lignification of loquat (*Eriobotrea japonica)* fruits through interaction with MYB TFs (Zeng *et al.*, 2015) and lignan biosynthesis

*These authors contributed equally to this work.

© 2019 The Authors
New Phytologist © 2019 New Phytologist Trust

in *Isatis indigotica* (Ma *et al.*, 2017). Conversely, though, an inhibitory effect on lignin deposition was observed by heterologous overexpression of the *Populus* homolog of *SHINE2* in tobacco (Liu *et al.*, 2017), calling for a deeper and wider analysis of this large TF family in lignification.

A genome-wide screen in *Populus trichocarpa* identified 170 gene models encoding ERFs (Vahala *et al.*, 2013). Expression of only a subset of ERFs was altered in response to aminocyclopropane-1-carboxylic acid (ACC) and ethylene treatment (Vahala *et al.*, 2013; Felten *et al.*, 2018). The dehydration-responsive element binding (DREB) subfamily member *ERF139* was one of the *ERF*s that was highly induced by ethylene (Vahala *et al.*, 2013) and by ACC (Felten *et al.*, 2018) in an ethylene-dependent manner, and it was shown to influence wood formation in transgenic trees (Vahala *et al.*, 2013). In the present study, we explored the role of ERF139 in xylem differentiation using transgenic overexpressor and dominant repressor lines. Our genetic approach revealed that ERF139 influences both xylem cell expansion and SCW chemistry. Transcriptional data from both types of transgenic lines supported the role of ERF139 in control of cell expansion and SCW formation, possibly by regulating a transcriptional response to cellular osmotic changes.

Materials and Methods

Plant material and growth conditions

All experiments were performed with hybrid aspen (*Populus tremula* L. × *P. tremuloides* Michx, clone T89). Plants were grown for 4 wk under *in vitro* conditions and subsequently transferred to 3 l pots (19 cm diameter) in a commercially available sand/soil/fertilizer mix (Krukjord; Hasselfors Garden, Örebro, Sweden) and grown for 6–7 wk in a glasshouse (18 h : 6 h, 20°C: 15°C, light : dark conditions, with relative humidity in the range 50–60%; metal halogen lamps). Growth conditions for trees used in the leaning experiments comprised 20°C: 15°C, light: dark temperatures and grown under LED lamps (FL300 Sunlight; Fiona Lighting, Sonderso, Denmark). Trees were fertilized once per week with *c.* 150 ml 1% Rika-S (N : P : K, 7 : 1 : 5; Weibulls Horto, Hammenhög, Sweden) starting in the week 3 after transplantation and ending 1 wk before harvest. All upright grown trees were rotated weekly to minimize positional effects. Material for Fourier transform-infrared spectroscopy (FT-IR), Klason lignin, monosaccharide analysis and pyrolysis GC-MS (Py/GC-MS) was collected at 10–15 cm above soil level. Bark and pith were removed from all stem pieces. Developing xylem was scraped from stem pieces 15–30 cm above soil and used to extract RNA for real-time quantitative PCR (qPCR) and RNA-sequencing (RNA-seq). Samples for wide-angle X-ray diffraction were obtained from stem pieces taken at 5–12 cm above soil.

Cloning and transformation of hybrid aspen

The *pLMX5::ERF139:SRDX* vector was amplified from the construct *pLMX5::ERF139* (Vahala *et al.*, 2013) which directs overexpression of the *P. trichocarpa ERF139* CDS (Potri.013G101100) from the wood-specific *LMX5* promoter (Love *et al.*, 2009). The promoter and gene sequence were amplified with the stop codon removed, using Phusion Hot Start High-Fidelity DNA Polymerase (Thermo Fisher Scientific, Waltham, MA, USA) and then cloned via pENTR/D-TOPO (pENTR Directional TOPO Cloning Kits; Invitrogen) to pHGEAR (Kubo *et al.*, 2005). This resulted in a C-terminal fusion with the ERF-associated amphiphilic repression (EAR) domain (SRDX; SUPERMAN repression domain X) (Hiratsu *et al.*, 2003). To study the ERF139 promoter (*pERF139*) activity, a 2103 bp promoter region was amplified from hybrid aspen (*Populus tremula* × *tremuloides*) genomic DNA, cloned into the pDONR221 donor vector and recombined to pKGWFS7, driving enhanced green fluorescent protein and β-glucuronidase (GUS) expression (Karimi *et al.*, 2002). The constructs were cloned into Agrobacterium strain GV3101 pMP90 followed by transformation of hybrid aspen (Nilsson *et al.*, 1992).

Selection of transgenic trees and qPCR

Expression of the *ERF139:SRDX* transgene was quantified from 12 independent lines by qPCR. Primers are listed in Table S7. RNA was extracted from stems of *in vitro*-grown trees using the CTAB method (Chang *et al.*, 1993), followed by lithium chloride precipitation and treatment with Ambion DNA-free DNase (Thermo Fisher Scientific). cDNA synthesis was carried out using the iScript cDNA Synthesis Kit (Bio-Rad). Five times diluted cDNA template was used for qPCR, using a Bio-Rad CFX96 Real Time System with SYBR Green Mastermix (Bio-Rad) and 5 pmol primers (Table S7). *PtACT1* (*Potri.001G309500*) served as a reference gene, selected because of its stable expression pattern in poplar stems (Wang *et al.*, 2016). *PtUBQ-L* served as a reference gene for confirmation of expression change of potential primary target genes. Expression of potential primary targets were tested in three biological replicates per line. Expression fold-change was calculated as $2^{-\Delta\Delta Ct}$ for each replicate. One WT replicate served as reference and its expression fold-change was subtracted from all other calculated expression fold-changes.

GUS analysis

Two representative transgenic lines carrying a p*ERF139*::*GUS* construct were selected from 14 lines based on their GUS activity, and grown in the glasshouse for 4 wk. Subsequently, trees were either grown for another 2 wk in the upright position or horizontally inclined (90°) to induce tension wood formation. Stem segments of *c.* 1.5 cm from 30 cm above soil level were used for histochemical staining. Samples were vacuum-infiltrated for 5 min and then incubated in a 1 mM X-GlcA, 50 mM K-phosphate buffer (pH 7.0), 0.1% Triton, 1 mM potassium ferricyanide and 1 mM potassium for 12 h at 37°C. The solution was replaced once after 3 h. Samples were then rinsed and cleared in an ethanol series. Samples were rehydrated and 70-μm-thick cross-sections (*c.* 400 μm below sample surface) were prepared using a vibratome. Micrographs were acquired using a Leica DMi8 inverted microscope with a 10X/0.32NA HC PL Fluotar semiapochromatic corrected objective with a high sensitivity color camera DFC7000 T (Mannheim, Germany).

© 2019 The Authors
New Phytologist © 2019 New Phytologist Trust

Histochemical staining and wood anatomy

Vibratome cross-sections (70 μm) of upright and leaned stems of ERF139OE and ERF139-SRDX trees were taken from the stems at 10 cm above the soil level, stained with Safranin : Alcian Blue (1 : 2), mounted in 50% glycerol and imaged with a Zeiss Axioplan2 microscope (Axiocam HRc camera and AxioVision v.4.8.2 software; Zeiss). Twenty times magnified images were utilized for quantification of total vessel lumen area in ImageJ (https://imagej.nih.gov/ij/). Images were first smoothed using a median filter and the signal was saturated. A threshold based on high signal intensity was applied for segmentation. To discriminate between fibers and vessels, vessel elements were always classified with a circularity larger than 0.3, but surface area thresholds had to be adjusted for each experiment.

Lignin autofluorescence was imaged in unstained cross-sections using a Leica DMi8 equipped with a DMC6200 camera (Leica, Mannheim, Germany). Quantification of fiber cross-sectional area was obtained using CellSet (Pound *et al.*, 2012) from pictures taken with ×100 magnification *c.* 1 mm inwards from the cambium (covering roughly 2000 μm^2). SCW thickness was determined on the same pictures in Fiji using the macro 'morpholibj' (Legland *et al.*, 2016). Images were made binary and cell walls were defined using the 'gray scale attribute filtering' option, in which black pixels represent the cell wall.

Fiber cross-sectional area and SCW thickness were also analyzed in high-resolution pictures using confocal laser scanning microscopy (CLSM) and transmission electron microscopy (TEM). CLSM images were acquired with a LSM800 microscope (Zeiss) using 488 nm laser excitation (4.5% power), a ×63 oil immersion lens (NA 1.4) and an Airyscan detector in super-resolution mode (wavelength detection window 500–700 nm). Images were taken *c.* 1 mm inwards from the cambium, covering a total area of *c.* 1600 μm^2. TEM pictures were taken with a Jeol 1230 transmission electron microscope and a Gatan MSC 600CW camera (Gatan Inc., Pleasanton, CA, USA). TEM pictures were taken from one biological replicate of WT and each transgenic line of the ERF139OE trees (covering an area of *c.* 2700 μm^2). Stem pieces were cut into 0.5-mm-thick sections by hand. Sections were incubated for at least 2 d in fixative (2.5% glutaraldehyde in 0.1 M sodium cacodylate buffer, pH 7.2). Before embedding in Spurr's resin (Spurr, 1969), sections were treated with 1% OsO_4 for 2 h, washed with distilled water and dehydrated using an ethanol wash series. After embedding, 60- to 90-nm-thick sections were obtained using an RMC Power Tome XL ultramicrotome (RMC; Boeckeler, Tucson, AZ, USA), substituted with a diamond knife (Diatome, Hatfield, PA, USA). The ultrathin sections were placed onto 100 mesh Ni-grids, incubated in 5% uranyl acetate in water for 20 min and subsequently stained with Sato's lead staining (Sato, 1968) for 5 min.

Wide-angle X-ray diffraction (WAXD)

Stem segments (5–12 cm above soil, 1 cm long) of three wild-type trees, one tree of each of the ERF139-SRDX lines 7, 8 and 15 and one tree of each of the ERF139OE lines 4 and 5, were debarked and sectioned with a microtome in the radial longitudinal direction. Wet 80-μm-thick sections were placed between two glass slides and dried under ambient conditions. The dry sections were mounted on aluminum frames and placed in a Bruker NanoStar device (Karlsruhe, Germany), equipped with an Incoatec ICT-IMS-CU X-ray tube (focal spot size of X-ray beam 115 μm, CuKa radiation, wavelength 1.54 Å) and a Vantec 2000 detector (2048 × 2048 pixels per frame; Billerica, MA, USA) with a sample detector distance of *c.* 90 mm. On each sample a line scan with a step size of 100 μm was performed throughout the entire diameter of the cross-section. Each measurement point was exposed to the beam for 60 min. The X-ray pattern was radially averaged from a *q*-range of 15.2–16.6 nm^{-1}, and the intensity was plotted over the azimuthal angle.

Wood chemistry analyses

Stem pieces of *c.* 2 cm in length were first debarked, split into half to remove the pith, freeze-dried and afterwards further split into smaller pieces with a razor blade and ground to a fine powder with a bead mill (MM400; Retsch, Haan, Germany). The dried wood powder was used for monosaccharide analysis, Py/GC-MS, FT-IR spectroscopy and Klason lignin analysis.

Monosaccharide (Ara, Rha, Fuc, Xyl, Man, Gal, Glc, GlcA and GalA) analysis by acid-catalyzed methanolysis was performed as described in Sweeley *et al.* (1963) using 500 ± 80 μg wood powder. Three biological replicates were analyzed for the WT and each transgenic line; 30 μg inositol was used as internal standard. Samples were vacuum-dried overnight at room temperature over a phosphorus pentoxide desiccant, following methanolysis for 24 h at 85°C using 2 M HCl/MeOH. Solvent was taken away and evaporated at 40°C. Samples were washed twice with normal methanol. Silylation was performed using Tri-sil reagent for 20 min at 80°C. After cooling down and removal of solvent, hexane was added and samples were centrifuged for 5 min at 18 000 ***g***. The solvent was filtered through a glass wool and a total volume of 100–200 μl was transferred in a GC microvial.

Lignin content was determined using Klason lignin (gravimetric method) as described in Sluiter *et al.* (2008) and Fengel & Wegener (2003). Briefly, 72% sulfuric acid was added to 10 ± 500 μg wood powder (three biological replicates and two technical replicates for each) and incubated at room temperature for 2 h. After addition of water, extraction of cell wall components continued for 2.5 h, and material was collected by centrifugation for 5 min at 2700 ***g*** and washed twice with water. Sample pellets were dried overnight at 103°C and analyzed for DW.

For Py/GC-MS, 60 ± 10 μg of ball-milled (MM400; Retsch) wood powder was applied to a pyrolyzer with an autosampler (PY-2020iD and AS-1020E; Frontier Lab, Fukushima, Japan) connected to a GC-MS (7890A/5975C; Agilent Technologies AB, Sweden). The analyses were done for minimum of three biological replicates in three replicates. Peak detection was done using the provided software (Chemstation; Agilent Technologies, Kista, Sweden). Peak calling and integration were performed as described by Gerber *et al.* (2012).

The FT-IR spectroscopy analysis was performed using 10 mg wood powder. FT-IR spectra for ERF139OE and the corresponding WT samples were extracted from Vahala *et al.* (2013).

© 2019 The Authors
New Phytologist © 2019 New Phytologist Trust

FT-IR analysis for ERF139-SRDX (and corresponding WT samples) was performed and analyzed exactly as described in Vahala *et al.* (2013). For data analysis, data from both experiments were combined. Data analysis for FT-IR included multivariate data analysis by orthogonal projection to latent structures-discriminant analysis (OPLS-DA; Trygg & Wold, 2002; Bylesjö *et al.*, 2006), performed in SIMCA 15.0 (Sartorius Stedim Biotech, Umeå, Sweden) on integrated peaks. In brief, OPLS-DA is a form of statistical modeling that, in our case, tries to predict genotypes (WT, ERF139OE or ERF139-SRDX) based on their wood chemical composition as measured by FT-IR. The prediction accuracy is evaluated by 'leave-one-out cross-validation', yielding a so-called Q^2 value ranging from 1 (perfect prediction accuracy) to $-\infty$. If the predicted value is high, it can be concluded that the cell wall chemical composition is different between the compared genotypes (meaning that genotypes can be predicted from their chemical composition). The loadings plot of the OPLS-DA indicates how much each measured chemical feature (each peak from FT-IR) correlates with the model that predictively discriminates between the genotypes. In all cases, at least three biological replicates per genotype and line were included.

Statistics

Mean, SE and *P*-values were calculated for growth parameters, SCW thickness, fiber cross-sectional area, vessel lumen area, cell wall composition and qPCR in R (v.3.4.2, BIOCONDUCTOR v.3.7) using a linear effect model (LME function in LIMMA, v.3.36.5), with genotype (and time in the case of tree growth data) as fixed effects. The MULTCOMPVIEW package (v.0.1-7) was used to assign statistically significant differences using a *P*-value cutoff of 0.05.

Gravitropic response following horizontal inclination

Trees for the leaning experiment were fertilized only up to 1 wk before inclination, to prevent additive effects on tension wood formation caused by high nitrogen fertilization (Pitre *et al.*, 2010). The leaning assay was performed separately for two lines each of ERF139OE and ERF139-SRDX, including respective WT, with at least three replicate trees in each experiment.

RNA-sequencing

RNA-sequencing data used in this manuscript were derived from two independent experiments. The first experiment included three independent transgenic lines (lines 4, 5 and 8) of the *pLMX5::ERF139* transgenic trees ('ERF139OE', material from three trees pooled per line) and two samples from the WT (material pooled from 10 trees for each). Each sample contained scraped material from the cambium and developing xylem from a stem piece taken from 15–30 cm above soil. RNA extraction was performed with the Bio-Rad Aurum Total RNA Minikit with 120 mg wood powder according to manufacturer's instructions. The remaining DNA was removed using Ambion DNAfree (ThermoScientific, Waltham, MA, USA) according to the manufacturer's instructions, followed by purification of the RNA using the MinElute kit (Qiagen). RNA quantity was checked by Nanodrop and quality by an RNA Agilent Bioanalyzer. Library generation and paired-end sequencing using Illumina HiSeq 2000 (San Diego, CA, USA) was performed by SciLifeLab (Science for Life Laboratory, Stockholm, Sweden). Raw data were deposited to the European Nucleotide Archive (ENA) under the accession PRJEB29149. The second RNA-seq experiment consisted of three WT and four independent transgenic lines of the *pLMX5::ERF139-SRDX* ('ERF139-SRDX'). Material was pooled from three trees per line. RNA extraction was done with the CTAB method followed by lithium chloride precipitation. All following steps were done as described earlier. Sequencing results for the ERF139-SRDX trees were deposited in the ENA under the accession PRJEB29150. Both datasets can be retrieved from the umbrella project PRJEB29153.

The *P. trichocarpa* genome was used for the alignment of quality-filtered and trimmed read pairs (genome sequence is available at Phytozome; Goodstein *et al.*, 2012). Read counting per gene and library was performed using HTSEQ (Anders *et al.*, 2015). Statistical data analysis was done in R (version 3.4.2) using DESEQ2 v.1.20 (Love *et al.*, 2014). This analysis included library size adjustment to obtain the size factor value for each genotype and variance stabilizing transformation (VST). Normalized read counts were used for differential gene expression analysis of ERF139OE and ERF139-SRDX in comparison to their respective WT. Overall similarity between all sequenced samples was assessed by principal component analysis (PCA). Differentially expressed genes (DEGs) between ERF139OE and WT (Table S2), as well as between ERF139-SRDX and its corresponding WT (Table S3), were selected using a $\log_2$fold-change ($|\log_2 FC| \geq 0.5$ and an adjusted *P*-value ≤ 0.05 as cutoffs (supported by Schurch *et al.*, 2016). Common DEGs from ERF139OE and ERF139-SRDX were obtained by intersecting the respective gene sets and visualized using the Venn diagram drawing tool available at http://bioinformatics.psb.ugent.be/webtools/Venn (Table S5). Gene names that do not start with '*Pt*' (for *P. trichocarpa*) are the names of the closest *A. thaliana* homologs. Heat maps were generated in R using the PHEATMAP package (v.1.0.10). Hierarchical clustering of genes was done with the default settings in PHEATMAP (clustering method 'single'). Gene promoter sequences (1 kb upstream of ATG) were extracted from http://popgenie.org (Sundell *et al.*, 2015). Motif enrichment and abundance were obtained using the MEME Suite programs (v5.0.5.) DREME (Bailey, 2011) and AME (McLeay & Bailey, 2010), respectively. Both programs were run with no changes to the preset settings. The custom scripts as well as their metadata are available from https://github.com/UPSCb/UPSCb/tree/master/manuscripts/Wessels2018.

Results

Overexpression of *Populus ERF139* in woody tissues negatively impacts tree growth

In order to elucidate the function of the *Populus* ERF139 during wood formation, growth and secondary xylem properties

© 2019 The Authors
New Phytologist © 2019 New Phytologist Trust

were analyzed in hybrid aspen trees that carried either a *P. trichocarpa ERF139* overexpressor construct ('ERF139OE') or a dominant repressor construct ('ERF139-SRDX'). Both constructs were expressed under the control of the wood specific *LMX5* promoter from *Populus tremula* × *tremuloides* gene *Potrx007740g00050* (Love *et al.*, 2009). Out of 12 lines, four ERF139-SRDX lines with the strongest transgene expression were selected for further experiments (Fig. S1). On the basis of the AspWood expression profile (Sundell *et al.*, 2017) of *LMX5* (Fig. 1a) and previous promoter activity studies (Love *et al.*, 2009), the *LMX5* promoter is known to be active during all stages of wood formation. According to the AspWood database, the expression of *ERF139* has a distinct peak of expression in the expanding xylem (Fig. 1a). Also transgenic hybrid aspen trees carrying a p*ERF139*::*GUS* construct revealed activity of the *ERF139* promoter in expanding and early differentiating xylem elements in addition to activity in the phloem (Fig. 1b). Taking into account the expression pattern of *ERF139*, transgene expression driven by the *LMX5* promoter is expected to extend the expression of *ERF139* and *ERF139-SRDX* substantially beyond the native *ERF139* expression domain during wood formation.

Four ERF139-SRDX and three ERF139OE lines were selected for detailed growth and wood anatomy analyses. In the two different types of transgenic trees, expression of *ERF139* was increased *c.* 180-fold compared with WT (Table S5), supporting equal expression levels of the transgenes. Plant height and stem diameter were recorded over a 5 wk growth period in the glasshouse (Fig. 1c,d). The ERF139OE trees showed reduced height growth and stem radial expansion both in the beginning (after 1 wk) and after 5 wk of growth as compared with the WT. The ERF139-SRDX trees did not show significant differences in stem height or diameter growth except for line 8, which had significantly increased height and stem diameter compared with WT after 5 wk of growth (Fig. 1c,d).

ERF139 promotes accumulation of guaiacyl (G)-type lignin

ERF139 was previously suggested to control SCW composition (Vahala *et al.*, 2013). FT-IR analysis of stem material showed that both the ERF139OE and ERF139-SRDX lines differed

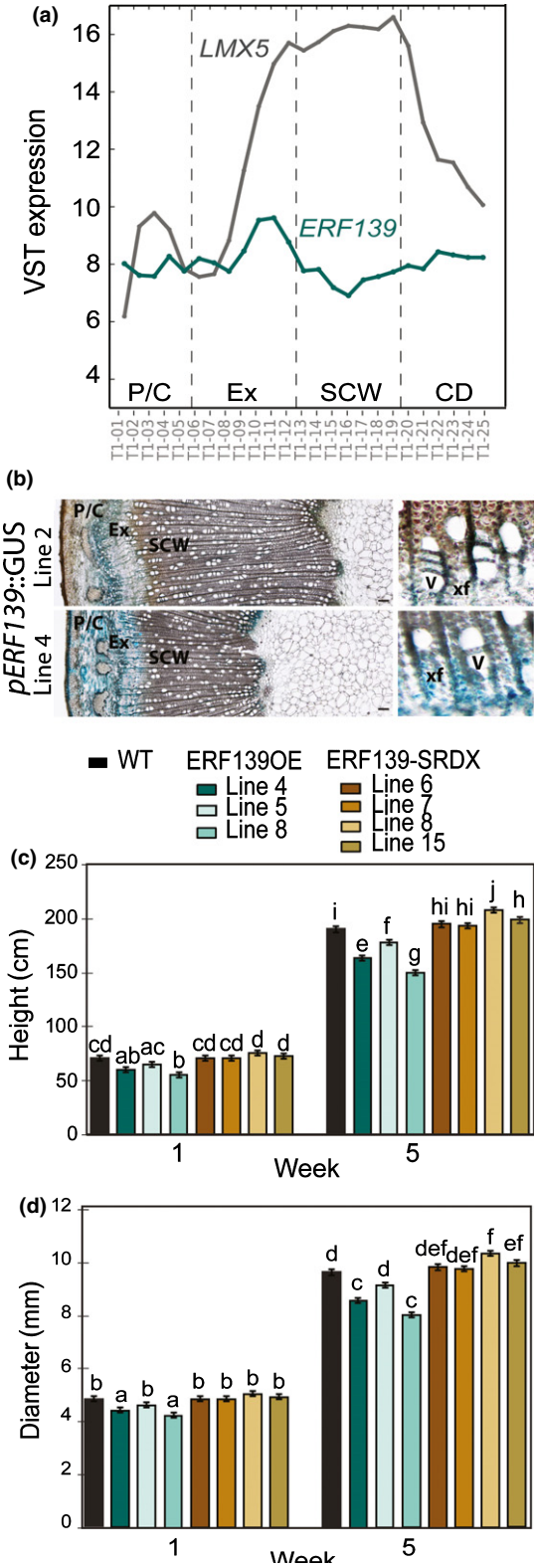

Fig. 1 *ERF139* overexpression restricts stem height and diameter growth in hybrid aspen. (a) Expression profile of *ERF139* and *LMX5* during wood development. Data were extracted from the AspWood database, which is based on RNA-sequencing data from longitudinal wood sections throughout the aspen stem (Sundell *et al.*, 2017). The corresponding *Populus trichocarpa* gene models *Potri.013G101100* (ERF139) and *Potri.002G101300* (LMX5) were used to retrieve the data from AspWood. Data are shown across all 25 sections from tree 1 (T1). P, phloem; C, cambium; EX, expanding xylem; SCW, secondary cell wall forming xylem; CD, programmed cell death zone. (b) β-Glucuronidase (GUS) staining in stems of two transgenic lines that express a p*ERF139*::*GUS* vector. The smaller images represent the area of the transition phase from xylem expansion to xylem maturation. v, vessel; xf, xylem fiber. Bar, 50 μm. (c, d) Tree height (c) and diameter (d) of wild-type (WT, black), *pLMX5::ERF139OE* (ERF139OE, green) and *pLMX5::ERF139-SRDX* (ERF139-SRDX, brown) trees after 1 and 5 wk growth in the glasshouse. Values are means ± SE of eight biological replicates calculated using a linear effect model with genotype and time as fixed effects. Statistical significance was assigned using a *P*-value cutoff of 0.05. Lines that do not share any letter are significantly different from each other.

© 2019 The Authors
New Phytologist © 2019 New Phytologist Trust

chemically from the WT (Fig. S2a). Comparative analyses (OPLS-DA) of the chemical spectra indicated that the ERF139OE lines differed from the WT with a high predictability ($Q^2 = 0.935$) whereas the ERF139-SRDX lines differed from the WT with lower predictability ($Q^2 = 0.765$) (Fig. S2b). Interestingly, the loadings plots revealed that vibrations typically associated with G-type lignin (at 1510 cm^{-1} for highly cross-linked lignin/monolignols and C=C stretches) were altered in opposite directions in the two different types of transgenic lines compared with the WT (Fig. S2b). These results suggest increased G-type lignin content in the ERF139OE and, contrastingly, decreased G-type lignin content in the ERF139-SRDX compared with the WT.

A more quantitative analysis of lignin chemistry was performed by two different methods. Klason lignin analysis showed increased overall lignin accumulation in the ERF139OE (by 53–77%) and up to 10–15% reduction in two ERF139-SRDX lines (Fig. 2a). Klason lignin does not, however, reveal changes in lignin composition, and we therefore analyzed the stem samples using Py/GC-MS, which allows relative quantification of the lignin monomers based on their respective MS peak area as a proportion of the total peak area (Gerber *et al.*, 2012). Py/GC-MS confirmed that the ERF139OE lines had increased relative content of G-lignin, and also indicated a significant reduction in the relative content of *p*-hydroxyphenol (H)-type lignin (Fig. 2b,c; Table S1). In contrast to the ERF139OE lines, the ERF139-SRDX lines showed a statistically significant decrease in the relative content of G-type lignin and an increase in H-type lignin in lines 6, 7 and 8. The predominant monolignol in angiosperm wood, syringyl (S)-type lignin, was not consistently affected in the ERF139OE or ERF139-SRDX lines (Fig. 2d), resulting in alterations in the S : G ratios (Fig. 2e) but only moderate changes in the total content of lignin in the ERF139OE and ERF139-SRDX lines (Fig. 2f).

The FT-IR analysis also supported effects of ERF139 on the carbohydrate components of the cell walls (vibrations 956-1140; Fig. S2). Monosaccharide analysis by acid-catalyzed methanolysis revealed changes in the abundances of xylose and glucose that were opposite in the ERF139OE and EFRF139-SRDX trees compared with the WT (Fig. 2g–o). These results suggest that ERF139 suppresses accumulation of glucose, derived from the amorphous cellulose and hemicellulose, and stimulates accumulation of xylose that is mainly derived from the hemicellulose xylan. Taken together, the opposite alterations observed in the wood chemistry of the ERF139OE and ERF139-SRDX lines suggest that ERF139 stimulates accumulation of G-type lignin and possibly the hemicellulose xylan, whereas it suppresses accumulation of the minor lignin component, the H-type lignin.

Overexpression of *ERF139* alters fiber and vessel cell morphology

Anatomical examination of stem cross-sections stained with Safranin-Alcian Blue indicated thicker SCWs and a general size reduction in the xylem fibers of ERF139OE trees compared with the WT (Fig. 3a). Quantification of fiber dimensions in images from light microscopy (Fig. 3a), epifluorescent microscopy (Fig. 3b–d), confocal microscopy (Fig. S3a) and TEM (Fig. S3b) confirmed these observations. Also vessel lumen area was reduced in ERF139OE lines 4 and 8 (Fig. 3e). Finally, WAXD analyses indicated higher microfibril angle and increased occurrence of the gelatinous (G) layer in the SCWs of the ERF139OE trees compared with the WT (Fig. S3c). Overexpression of *ERF139-SRDX* did not result in changes in xylem cell morphology compared with WT, except for the vessel diameter, which was significantly larger of in the ERF139-SRDX line 8 than in the WT (Fig. 3e).

Enhanced ethylene signaling highlights the function of ERF139 in suppressing vessel expansion

The fact that the dominant repressor lines had only a subtle effect on tree growth and xylem cell morphology could be a result of the requirement for increased ethylene biosynthesis and/or signaling, as *ERF139* is known to be induced by ethylene (Vahala *et al.*, 2013). Because a genetic approach to this question is difficult in hybrid aspen, we decided to expose the WT and two representative lines of ERF139OE and ERF139-SRDX to a gravitational stimulus by inclining trees (90°) over a 2- (Fig. 4a) or 4-wk period (Fig. 4b–g) – a condition well known to stimulate ethylene biosynthesis and signaling in the SCW zone (Andersson-Gunnerås *et al.*, 2003; Love *et al.*, 2009). GUS staining of the transgenic lines carrying the p*ERF139:.GUS* construct revealed similar but possibly somewhat stronger activity of the *ERF139* promoter in the inclined stems (Fig. 4a) compared with the upright-grown stems (Fig. 1b). Safranin-Alcian Blue staining of sections from the inclined stems supported enhanced overall lignification and SCW thickness in the tension wood side of the ERF139OE trees (Fig. 4c,d). Quantification of the lignified SCW area indicated increased SCW thickness on the tension wood side of the stem in the two ERF139OE lines and decreased SCW thickness in the ERF139-SRDX lines, even though statistically significant changes were found only in line 8 (Fig. 4e). Xylem vessel lumen area was significantly lower in the ERF139OE, and larger in the ERF139-SRDX lines, compared with the WT on both the tension and opposite wood sides of inclined stems (Fig. 4f). No changes were observed for xylem fiber cross-sectional area in either the opposite or the tension wood side of the stems (Fig. 4g). Therefore, the experimental setup adopted here validated the function of ERF139 in suppressing vessel expansion, and also supported a function in determining the overall SCW thickness, at least under conditions of enhanced ethylene signaling.

ERF139 targets a large number of TFs

To unravel the regulatory cascades underlying the phenotypes observed in the ERF139OE and ERF139-SRDX trees, xylem transcriptomes were analyzed in both genotypes using RNA-seq. Unconstrained PCA of the RNA-seq data separated the wood transcriptomes according to their genotypic background (component 1; Fig. S4a). The genotype explained 41% and 45% of the

© 2019 The Authors
New Phytologist © 2019 New Phytologist Trust

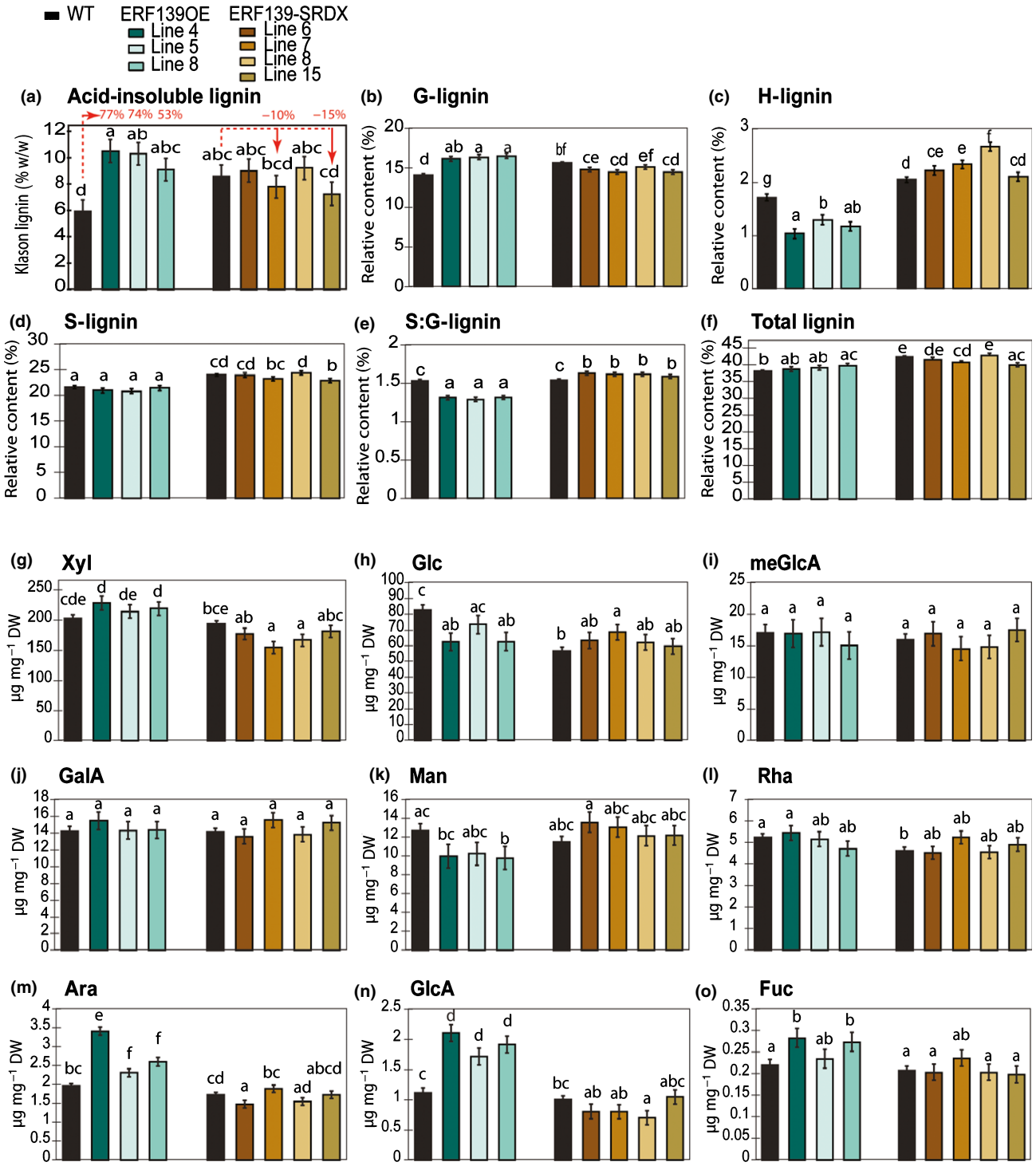

Fig. 2 ERF139 promotes accumulation of G-type lignin in hybrid aspen secondary xylem tissues. (a) Klason lignin content. The data are means ± SE from three biological replicates per line calculated using a linear effect model with genotype as the fixed effect. Statistical significance was assigned using a *P*-value cutoff of 0.05. Lines that do not share any letter are significantly different from each other. (b–f) Pyrolysis/GC-MS (Py/GC-MS) data showing relative content (to the total peak area) of guaiacyl (G)-type lignin (b), *p*-hydroxyphenol (H)-type lignin (c), syringyl (S)-type lignin (d), S : G-type lignin ratio (e) and total lignin in wild-type (WT), ERF139OE and ERF139-SRDX (f). Data are means ± SE of at least three biological replicates (three for ERF139OE lines, four for ERF139-SRDX lines, nine for WT samples used for the comparison with ERF139OE and 16 for WT samples used for comparison of ERF139-SRDX samples). Means ± SE were calculated using a linear effect model with genotype as fixed effect and statistically significant differences were marked using a *P*-value cutoff of 0.05. Raw data from Py-GC-MS can be found in Supporting Information Table S1. (g–o) Monosaccharide content. Means ± SE of each monosaccharide are calculated from at least three biological replicates (three for ERF139OE lines, four for ERF139-SRDX lines, nine for WT samples used for the comparison with ERF139OE and 16 for WT samples used for comparison of ERF139-SRDX samples). Xyl, xylose; Glc, glucose; meGlcA, methyl glucuronic acid; GalA, galacturonic acid; Man, mannose; Rha, rhamnose; Ara, arabinose; GlcA, glucuronic acid; Fuc, fucose. Means ± SE were calculated using a linear effect model with genotype as fixed effect. Lines that do not share any letter are significantly different from each other using a *P*-value cutoff of 0.05.

© 2019 The Authors
New Phytologist © 2019 New Phytologist Trust

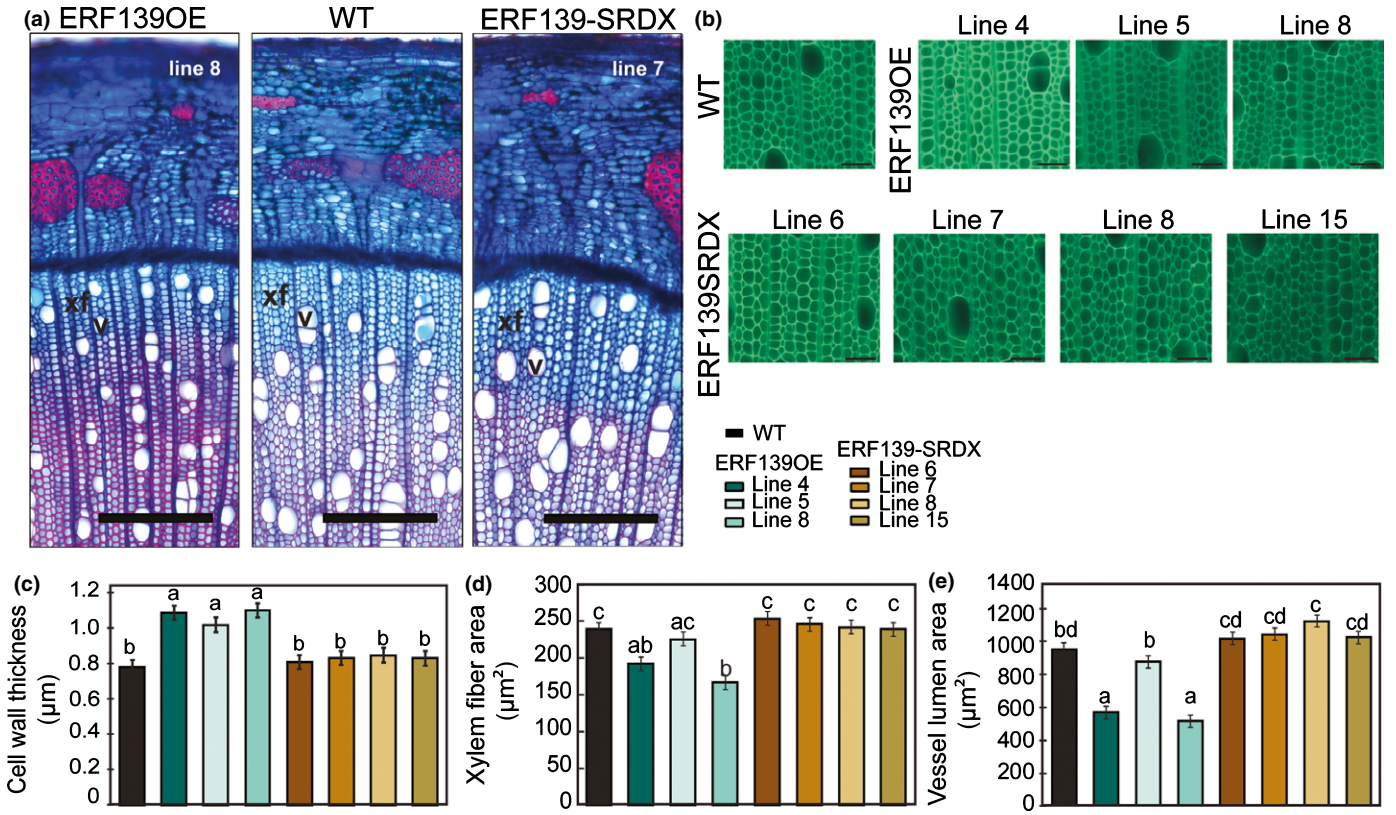

Fig. 3 Overexpression of *ERF139* affects secondary cell wall (SCW) thickness and xylem cell size in hybrid aspen. (a) Stem cross-sections of ERF139OE (line 8), wild-type (WT) and ERF139-SRDX (line 7) stained with Safranin-Alcian Blue which stains lignin red and matrix polysaccharides blue. Bar, 250 μm. Xf, xylem fiber; v, vessel element. (b) Secondary xylem tissues in stem cross-sections taken from WT, ERF139OE (lines 4, 5 and 8) and ERF139-SRDX (lines 6, 7, 8 and 15). Lignin autofluorescence was imaged for each line at three different positions at a distance of *c.* 1 mm from the vascular cambium, and used for the measurements in (c) and (d). Bar, 20 μm. (c) Cell wall thickness. (d) Xylem fiber cross-sectional area. (e) Cross-sectional vessel lumen area measured from pictures shown in (a). The values are means ± SE of three biological replicates using a linear effect model with genotype as a fixed effect. Lines that do not share any letter are significantly different from each other using a *P*-value cutoff of 0.05.

transcriptome differences in ERF139-SRDX and ERF139OE, respectively, compared with the WT. Next, we selected DEGs in ERF139OE vs WT (Table S2) and in ERF139-SRDX vs WT (Table S3) using $|\log_2 FC| \geq 0.5$ and adjusted $P \leq 0.05$ cutoffs. In all, 740 DEGs were identified for ERF139OE with a near equal distribution of up- and downregulated genes (382 and 353, respectively) (Fig. 5a). A slightly higher number of DEGs (956) was identified for ERF139-SRDX, also with a near-equal distribution of up- and downregulated genes (464 and 492, respectively). To identify secondary growth-related processes that show differential regulation in the ERF139OE and the ERF139-SRDX lines, DEGs were assigned to transcriptional modules that were associated with cambial cell division, cell expansion, secondary wall deposition, lignification, and cell death in the AspWood dataset (Sundell *et al.*, 2017; Fig. S4b; Table S4). The ERF139OE trees showed a high frequency of DEGs associated in AspWood with proteolysis, glycolysis and SCW biosynthesis, whereas DEGs in the ERF139-SRDX trees represented genes that were associated in AspWood, for instance, with biological processes of cell expansion and pectin modification (Fig. S4b; Table S4). To differentiate between the direct and indirect functions of ERF139, we categorized DEGs that were common among the induced or suppressed DEGs of the ERF139OE and the suppressed DEGs of the ERF139-SRDX trees as 'primary' targets (Fig. 5b; Table S5). As the SRDX domain turns ERF139 into an active repressor, direct targets of ERF139 have to be suppressed in ERF139-SRDX (Fig. S4c,d). In all, 88 of the DEGs fulfilled our criteria of a primary target gene (Fig. 5c). Expression of four primary targets (*ABA DEFICIENT1* (*ABA1*), *LACCASE5* (*LAC5/PtLAC26*), *LOB DOMAIN-CONTAINING PROTEIN15* (*LBD15*) and *MYB86*) were validated in xylem samples from an independent growth trial by qPCR (Fig. 5d). Most of the primary target genes (78) were induced in ERF139OE and repressed in ERF139-SRDX (Fig. 5c), suggesting that ERF139 mainly functions as an activator of gene expression.

Primary target genes were enriched in AP2/ERF-domain TFs (e.g. *TOE1*, *PtERF36*, *PtERF45*, *PtERF48* and *PtERF108*; Fig. 5c; Table S5). Accordingly, motif enrichment tests in promoter regions (1 kb upstream) of primary targets revealed a significant enrichment ($P < 0.01$) of two motifs bound by ERFs: the GCC-Box ('GCCGCC') and the dehydration response element (DRE; 'RCCGAC'; Fig. 5c; Table S5) which is bound by AP2-domain family members that belong to the CBF/DREB

© 2019 The Authors
New Phytologist © 2019 New Phytologist Trust

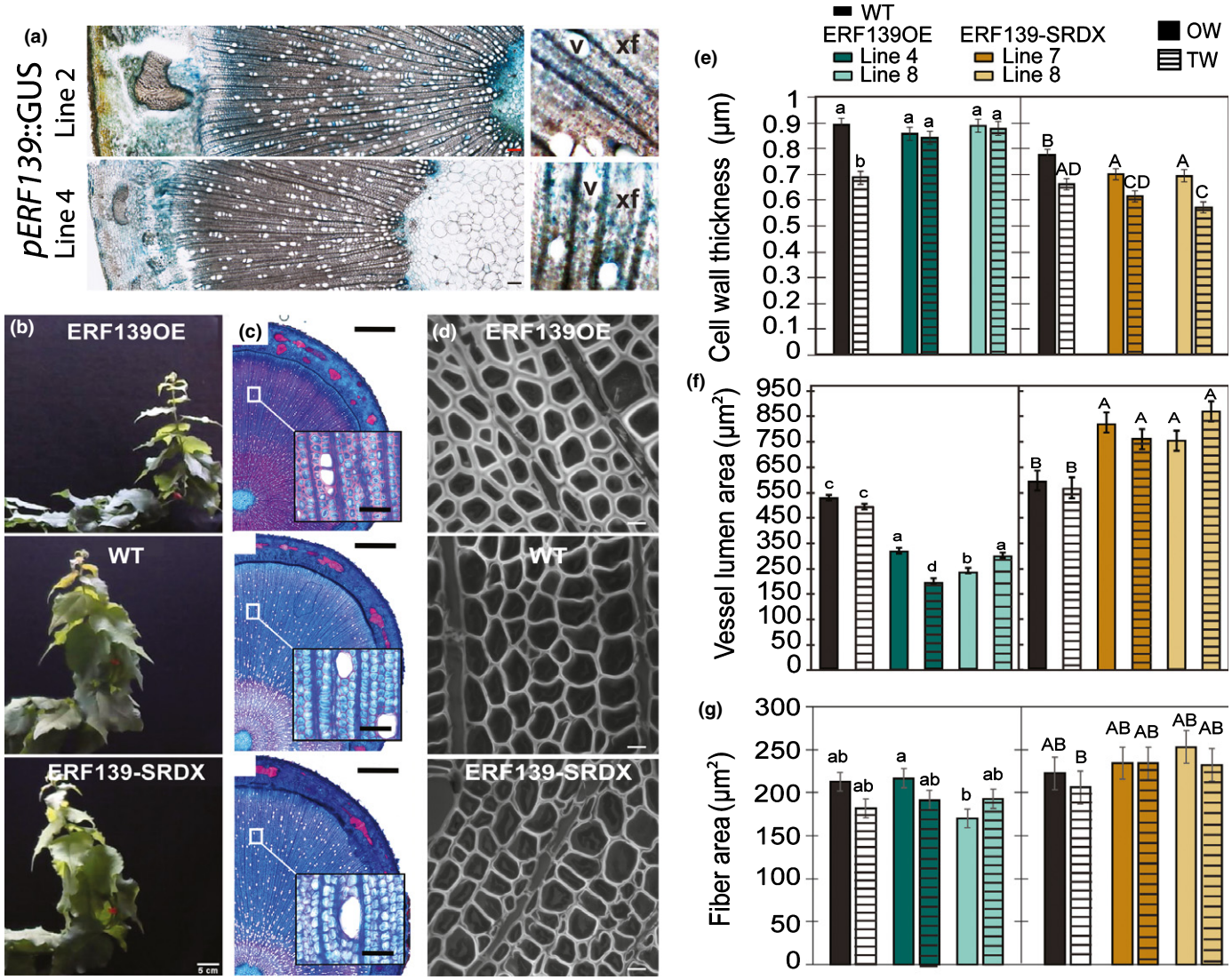

Fig. 4 ERF139 impedes vessel expansion in inclined transgenic hybrid aspen trees. (a) β-Glucuronidase (GUS) staining in inclined stems of transgenic hybrid aspen trees carrying a *pERF139::GUS* construct. Trees were horizontally inclined for 2 wk. The smaller images represent the transition phase from xylem expansion to xylem maturation. xf, xylem fiber; v, vessel. Bar, 50 μm. (b) Stem lift at 21 d after leaning of ERF139OE (line 8, top panel), wild-type (WT, middle panel) and ERF139-SRDX (line 7, bottom panel) trees. Bar, 5 cm. (c, d) Images of cross-sections from tension wood of stems at 4 wk after inclination of the trees. Sections were stained with Safranin-Alcian Blue to visualize xylem cell sizes and lignification, and detected by bright field microscopy (c) or by epifluorescence microscopy (d). Bars: (c) 1 mm in the upper right corner and 50 μm in the magnified images; (d) 10 μm. (e) Cell wall thickness. (f) Cross-sectional vessel lumen area in tension wood (TW, bars with pattern) and opposite wood (OW) of WT, ERF139OE and ERF139-SRDX trees. (g) Cross-sectional fiber area. Quantifications in (e–g) were performed on the kind of images shown in (d) in an area *c*. 1 mm from the vascular cambium. Data are means ± SE from four biological replicates calculated by a linear model with genotypes as fixed effect. Statistically significant differences were assigned using a *P*-value cutoff of 0.05.

subgroup (Sun *et al.*, 2008). We identified the DRE-motif and/or the GCC-box in the promoters of three TFs (*PtERF48*, *TOE1*, *ANAC2)*, but also genes that are related to processes such as cell wall metabolism (UDP-D-glucose/UDP-D-galactose 4-epimerase 2 (*UGE2*) and *pectin lyase*), and abiotic (e.g. *ABA1*, *RHY1A*) and biotic stresses (e.g. *MLO4*, *LRR protein* (*Potri.011G13970*); Table S5). We also identified the enrichment of the G-Box ('CACGTG') and an R2R3-type/MYB-related motif ('TWGKTR' (Agarwal *et al.*, 2006); Fig. 5c; Table S5). Several primary targets ($n = 27$) that contained the G-box or the Myb-related motif also contained either the GCC-box or the DRE-motif. We next addressed the role of ERF139 on transcriptional regulation of lignin biosynthesis and polymerization (Figs 5e, S4e; Table S6). The primary targets contained *LAC5* and two TFs (*MYB86, ERF9* (*PtERF45*)) that were earlier shown to bind to promoters of lignin-biosynthetic genes *in vitro* in Arabidopsis (Taylor-Teeples *et al.*, 2015). Although only a few of the lignin-biosynthetic genes were differentially expressed in ERF139OE and ERF139-SRDX, several genes that encode laccases and peroxidases were differentially expressed, especially in the ERF139OE but without any preferential direction in expression (Figs 5e, S4e; Table S6).

© 2019 The Authors
New Phytologist © 2019 New Phytologist Trust

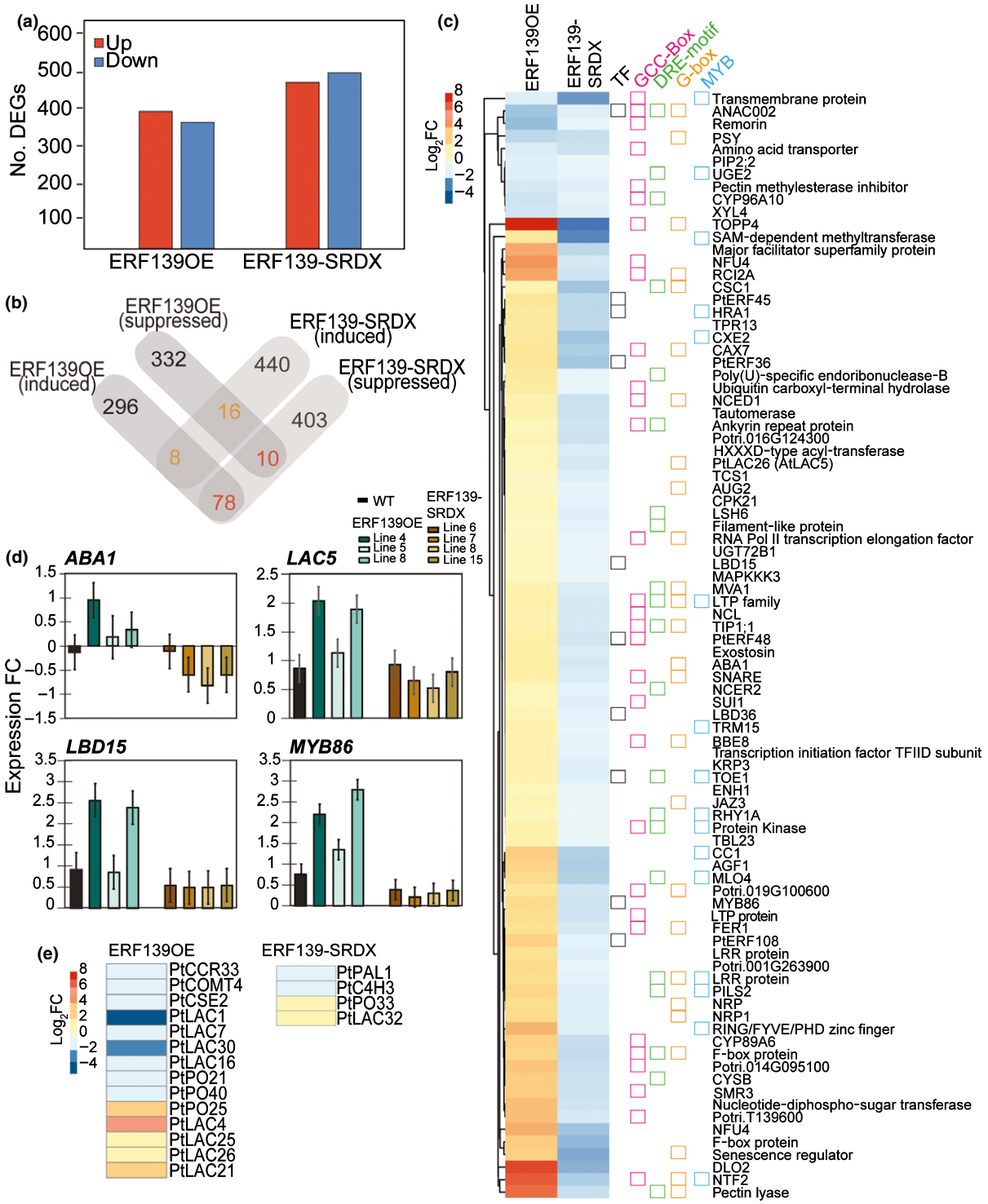

Fig. 5 Comparative transcriptome analysis of ERF139OE and ERF139-SRDX hybrid aspen trees. (a) Bar graphs showing the number of differentially expressed genes (DEGs) that are up- (red) and downregulated (blue) in ERF139OE and ERF139-SRDX compared with the wild-type (WT). (b) Venn diagram showing shared DEGs between ERF139OE and ERF139-SRDX (see Supporting Information Table S5). For further analysis, DEGs that are suppressed in ERF139-SRDX and are among the DEGs of ERF139OE are defined as 'primary' gene targets of ERF139 (highlighted in red). (c) Heat map showing the expression profile as a $\log_2$fold-change ($\log_2$FC) in all primary target genes of ERF139 in ERF139OE and ERF139-SRDX. Red indicates gene induction, and blue indicates gene suppression compared with WT. Transcription factors are marked with a black box. Presence of enriched motifs (including the GCC-box 'GCCGCC', the DRE-motif 'RCCGAC', the G-box 'CACGTG' and a Myb-related motif 'TWGKTR') in promoter regions (1000 bp) of primary targets are indicated with pink, green, yellow and blue green boxes, respectively. (d) Relative expression of four primary targets (*ABA1*, *LAC5*, *LBD15*, *MYB86*) as fold-change relative to *UBQ-L* in WT (black), ERF139OE (green) and ERF139-SRDX (brown) trees. Means ± SE were calculated from three biological replicates per genotype using a linear effect model with genotype as fixed effect. (e) Heat map showing expression changes ($\log_2$FC) of lignin-related DEGs in ERF139OE and ERF139-SRDX compared with the WT (for a more detailed description, see Table S6).

© 2019 The Authors
New Phytologist © 2019 New Phytologist Trust

ERF139 target genes indicate involvement of osmotic changes in the transition phase between xylem cell expansion and SCW formation

The primary targets include only a few genes previously described in xylem differentiation. ERF139 stimulated expression of *LBD15* (Fig. 5c,d), which has been shown to regulate tracheary element differentiation in Arabidopsis (Ohashi-Ito *et al.*, 2018) and to activate promoters of PtrCesA8, PtrGT43B, PtrGT47A and PtrCCoCAOMT1 in *P. trichocarpa* (Zhong *et al.*, 2011), *LAC5*, which might be involved in lignification, and UDP-glycosyltransferase 72B1 (UGT72B1), which catalyzes monolignol conjugation in Arabidopsis (Lin *et al.*, 2016). They all have their highest expression during early stages of SCW formation according to the AspWood database (Figs 6, S5).

Expression of the primary gene targets of ERF139 was highly interconnected in the AspWood network (Figs 6, S5). *ERF139* was coexpressed with *MYB86* and *DOWNY MILDEW RESISTANT6-LIKE OXYGENASE2* (*DLO2*), both showing their highest expression during the transition phase between xylem expansion and SCW formation (Figs 6, S5). Primary targets with most connections (edges) in the network (connections to at least seven other primary target genes) included an ankyrin repeat family protein, an *LTP* (*lipid transfer protein*), *ABA1* and *TIP1;1* (*TONOPLAST INTRINSIC PROTEIN1;1*), which are all highly expressed in expanding xylem cells before the onset of SCW formation, similar to *ERF139* (Figs 6, S5). On the basis of their network centrality and expression pattern in AspWood they are expected to have central roles in xylem expansion and SCW formation together with ERF139.

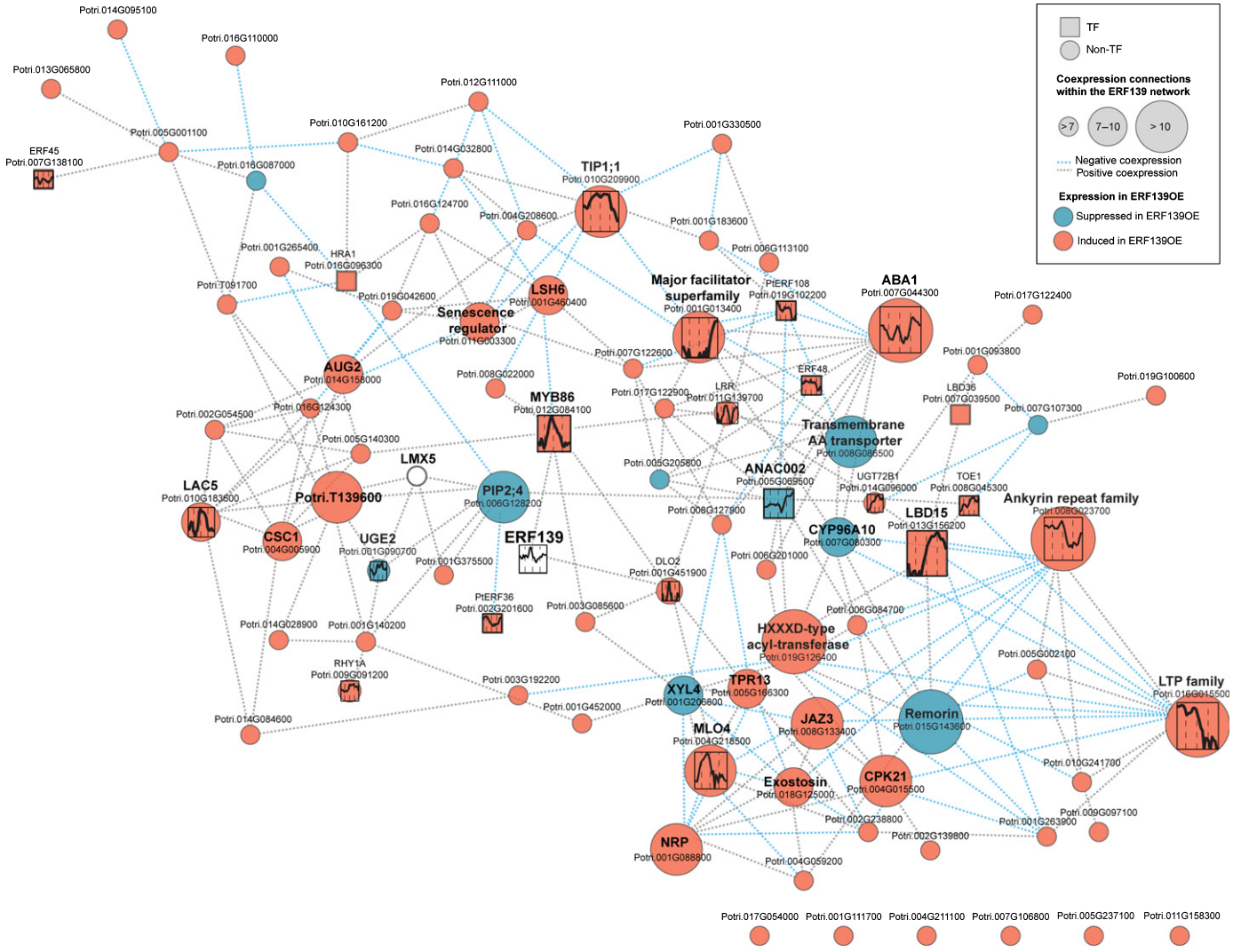

Fig. 6 ERF139 primary target coexpression network in wood formation in hybrid aspen. Coexpression network of primary targets of ERF139 during wood formation. Data (variance stabilizing transformation expression) was extracted from the AspWood database (Sundell *et al*., 2017). The network also includes *ERF139* and *LMX5*. Gene expression in ERF139OE is indicated by the background color of each square (representing a transcription factor) or circle; blue indicating suppression and red induction in ERF139OE. Negative correlation between gene expression in AspWood is indicated by blue dashed lines, and positive correlation by grey lines. Genes with at least seven connections within the network are highlighted by enlarged circles/squares. AspWood expression profiles are shown for all genes mentioned in the text. Dashed lines within the AspWood gene expression profile indicate transition between phloem/cambium, expanding xylem, secondary cell wall (SCW) formation and cell death (as shown in Fig. 1a).

© 2019 The Authors
New Phytologist © 2019 New Phytologist Trust

As suggested by the induction of *ABA1* in ERF139OE (Fig. 5c,d) and coexpression with *ABA1* in AspWood (Figs 6, S5), ERF139 might activate ABA biosynthesis during the transition between xylem expansion and initiation of SCW formation. ABA1 has been implicated in the regulation of xylem fiber differentiation (Campbell *et al.*, 2018), but is primarily recognized as a key regulator of ABA-mediated osmotic stress response (Chen *et al.*, 2005; Hernández-Blanco *et al.*, 2007). We therefore investigated the expression of the ERF139 primary targets upon osmotic stress, utilizing publicly available transcriptomic datasets from *Populus* (Janz *et al.*, 2012; Xue *et al.*, 2016; Yu *et al.*, 2017). Expression of *c.* 82% of the primary targets was affected in at least one of the analyzed conditions (Fig. S5; Table S5). Furthermore, out of the 26 most central genes in the network of the primary targets (in Fig. 6), expression of 22 genes was changed upon osmotic changes in samples from the phloem and/or xylem tissues (Fig. S5). Most of the primary targets that showed changes in expression under drought and salt stress also showed their highest expression in the transition phase between xylem expansion and SCW initiation (e.g. *ERF139*, *MYB86*, *MLO4*, *LTP family protein*, *Ankyrin repeat family*) or SCW formation itself (e.g. *LAC5*, *TIP1;1*, *LBD15*) in AspWood. These results collectively suggest that osmotic changes occur during xylem differentiation, and that ERF139 controls a transcriptional network that is responding to these changes.

Discussion

Our results demonstrate that ERF139 is a key factor within a regulatory cascade that controls vessel expansion. Overexpression of *ERF139* in all xylem cell types (by the wood-specific *LMX5* promoter) resulted in reduced radial dimensions of both xylem fibers and vessel elements (Fig. 3d,e). However, dominant repression of ERF139 function in the ERF139-SRDX trees supported a role of ERF139 specifically in the expansion of vessel elements. Although the effect was indicated by results in only one of the ERF139-SRDX lines in the upright grown trees, increased vessel expansion was obvious in all ERF139-SRDX lines that were exposed to conditions stimulating ethylene biosynthesis and signaling (Fig. 4f). It seems possible, therefore, that the role of ERF139 in modulating vessel expansion is imperative in conditions of enhanced ethylene signaling, such as gravitropic stimulation of the stem.

In addition to vessel expansion, ERF139 also influenced SCW chemistry (Figs 2, S2). The transgenic overexpression and dominant repressor lines suggested that ERF139 stimulates accumulation of the G-type lignin and suppresses the H-type lignin (Fig. 2a–f). The transcriptomic analyses supported a direct function of ERF139 on lignin biosynthesis because at least three lignin-related genes (*LAC5*, *UGT72B1* and *MYB86*) were identified as putative direct targets of ERF139 (Fig. 5c). The *LAC5* homolog in *Arabidopsis* has an expression pattern that is consistent with a role in lignification (Berthet *et al.*, 2011). UGT72B1, which catalyzes glucose conjugation of monolignols, has been shown to influence monolignol availability and hence lignification in *Arabidopsis* (Lin *et al.*, 2016). Expression of *MYB86* is highly coregulated with *ERF139* in AspWood (Figs 6, S5), and the homologous gene in *Arabidopsis* has been shown to bind to promoter regions of several lignin-biosynthetic genes in a yeast one-hybrid screen (Taylor-Teeples *et al.*, 2015; Kumar *et al.*, 2016). But ERF139 also influenced carbohydrate composition of the SCWs (Fig. 2g–o), and the ERF139OE lines showed massively thickened cell walls (Figs 3c, S3a,b), suggesting that ERF139 stimulates the whole SCW deposition program. This was supported by the fact that a homolog of *NST1*, and homologs of two other TFs known to control xylem differentiation, *VND1* and *LBD15* (Zhong *et al.*, 2007; Zhou *et al.*, 2014; Ohashi-Ito *et al.*, 2018), were upregulated in the *ERF139*-overexpressing lines (Table S2). Even though functional characterization of these multigene families of TFs in *Populus* spp. is still required, it appears that ERF139 may function as an upstream component that activates some of the regulators of the SCW biosynthetic pathway.

The fact that ERF139 influences both xylem vessel cell expansion and SCW formation suggests that the effect of ERF139 on these two processes is interlinked. *ERF139* is induced specifically at the end of xylem cell expansion and when SCW biosynthesis is initiated (Fig. 1a), pointing towards a role of ERF139 in controlling the transition between these two phases. Little is known about regulation of this transition phase, but it has been shown that precocious maturation of xylem vessel elements can lead to decreased cell sizes (Muñiz *et al.*, 2008; Zhao *et al.*, 2008). Enhanced or precocious SCW formation in the ERF139OE lines might therefore prevent full radial expansion of vessel elements, and vice versa in the case of the ERF139-SRDX. Our results suggest that accumulation of G-type lignin, and/or the likely increase in xylan, could be central to ending the phase of xylem vessel expansion and hence determining the size of the vessel elements.

The transcriptome analyses offered an insight into possible mechanism on how ERF139 might regulate the transition between cell expansion and SCW deposition. Expression of most of the putative direct targets, as well as *ERF139* itself, have in previous studies been shown to respond to either drought or increased salinity (Fig. S5; Table S5). Many of them, including *ABA1*, *Cystatin B*, *the GPI-anchored adhesin-like protein TRM15* (*TON1 RECRUITING MOTIF 15*) and *DLO2* are coexpressed with *ERF139* during the transition phase between cell expansion and initiation of SCW formation (Fig. S5), suggesting that conditions resembling drought and/or salt stress prevail during the transition to SCW formation. Overexpression of DREB-type AP2/ERFs has been shown to increase tolerance to osmotic stress, but to affect plant height negatively and often result in dwarf plants (Zhang *et al.*, 2009; Zhou *et al.*, 2012; Lee *et al.*, 2016; Kudo *et al.*, 2017). The stunted growth phenotype of ERF139OE trees (Fig. 1c,d) suggests that overexpression of *ERF139* triggers a transcriptional response and morphological changes similar to those induced in response to osmotic stress. Indeed, wood formed in *Populus* under salt and drought stress displayed, similar to the ER139OE trees, a general reduction in vessel lumen, an increase in vessel density and induction of lignin biosynthesis (Janz *et al.*, 2012). Therefore, it seems likely that at the late stage of xylem expansion, cells experience drastic changes

© 2019 The Authors
New Phytologist © 2019 New Phytologist Trust

in osmotic potential. The function of ERF139 might be required at this stage to coordinate transition between cell expansion and SCW deposition in response to these changes.

Acknowledgements

We are grateful to Dr Matthew Zinkgraf for assistance with the leaning experiments. We thank Daniel Werner for excellent assistance in the microfibril angle measurement, Björn Sundberg for the initial contribution to the project, and Ewa Mellerowicz for helpful discussions. The project was funded by the Swedish Research Council Formas (grant nos. 213-2011-1148 and 239-2011-1915), the Kempe foundations (grant nos. SMK-1649 and SMK-1533), The Swedish Foundation for Strategic Research (RBP14-0011), the Sven och Lilly Lawski stiftelsen, the Swedish Governmental Agency for Innovation Systems (grant no. 2016-00504), the KAW Foundation (grant no. 2016-0341) and the Federal Ministry of Education and Research BMBF (grant no. 033L055). Sequencing was performed by the SciLife Lab (Stockholm, Sweden) and data storage was provided by the Swedish National Infrastructure for Computing (SNIC) at UPPMAX. We also thank the KBC Biopolymer Analysis platform, supported by Bio4Energy and the TC4F project, the Vibrational Spectroscopy Core Facility, supported by the Department of Chemistry and the Chemical Biological Centre (KBC) of Umeå University, and the Umeå Core Facility for Electron Microscopy at Umeå University. HT is a member of the holding company Woodheads AB, a part-owner of SweTree Technologies, which played no part in this work.

Author contributions

BW, JF, JK and HT designed the experiments. TV wrote the macro for determination of the vessel lumen area. BW generated the ERF139-SRDX construct and transgenic lines, and performed the growth, histology, GUS and tension wood experiments. BW and CS performed assays for xylem chemistry. CS performed quantification of fiber cross-sectional area and SCW thickness and all bioinformatic analyses. SE and JF performed CLSM and TEM, respectively. ND helped with the RNA-seq analysis. JV performed recombinant DNA work. ME performed the WAXD experiments. BW, CS, SE and KA analyzed the data. BW and CS discussed the data. BW, CS and HT wrote the manuscript with contributions from all co-authors.

ORCID

Nicolas Delhomme https://orcid.org/0000-0002-3053-0796
Michaela Eder https://orcid.org/0000-0002-1461-1668
Sacha Escamez https://orcid.org/0000-0001-7049-6978
Judith Felten https://orcid.org/0000-0002-0444-822X
Jaakko Kangasjärvi https://orcid.org/0000-0002-8959-1809
Carolin Seyfferth https://orcid.org/0000-0002-8962-3778
Hannele Tuominen https://orcid.org/0000-0002-4949-3702
Thomas Vain https://orcid.org/0000-0002-8153-907X
Bernard Wessels https://orcid.org/0000-0003-0717-1630

References

Agarwal M, Hao Y, Kapoor A, Dong CH, Hiroaki F, Zheng X, Zhu JK. 2006. A R2R3-type MYB transcription factor is involved in the cold-regulation of CBF genes and in acquired freezing tolerance. *Journal of Biological Chemistry* **49**: 37636–37645.

Ambavaram MM, Krishnan A, Trijatmiko KR, Pereira A. 2011. Coordinated activation of cellulose and repression of lignin biosynthesis pathways in rice. *Plant Physiology* **155**: 916–931.

Anders S, Pyl PT, Huber W. 2015. HTSeq—a Python framework to work with high-throughput sequencing data. *Bioinformatics* **31**: 166–169.

Andersson-Gunneras S, Hellgren JM, Björklund S, Regan S, Moritz T, Sundberg B. 2003. Asymmetric expression of a poplar ACC oxidase controls ethylene production during gravitational induction of tension wood. *The Plant Journal* **34**: 339–349.

Bailey TL. 2011. DREME: motif discovery in transcription factor ChIP-seq data. *Bioinformatics* **27**: 1653–1659.

Berthet S, Demont-Caulet N, Pollet B, Bidzinski P, Cézard L, Bris PL, Borrega N, Hervé J, Blondet E, Balzergue S *et al.* 2011. Disruption of LACCASE4 and 17 Results in Tissue-Specific Alterations to Lignification of *Arabidopsis thaliana* Stems. *Plant Cell* **23**: 1124–1137.

Bylesjö M, Rantalainen M, Cloarec O, Nicholson JK, Holmes E, Trygg J. 2006. OPLS discriminant analysis: combining the strengths of PLS-DA and SIMCA classification. *Journal of Chemometrics* **20**: 341–351.

Campbell L, Etchells JP, Cooper M, Kumar M, Turner SR. 2018. An essential role for abscisic acid in the regulation of xylem fibre differentiation. *Development* **145**: dev161992.

Chang S, Puryear J, Cairney J. 1993. A simple and efficient method for isolating RNA from pine trees. *Plant Molecular Biology Reporter* **11**: 113–116.

Chen Z, Hong X, Zhang H, Wang Y, Li X, Zhu JK, Gong Z. 2005. Disruption of the cellulose synthase gene, AtCesA8/IRX1, enhances drought and osmotic stress tolerance in *Arabidopsis*. *The Plant Journal* **43**: 273–283.

Chen H, Wang JP, Liu H, Li H, Lin YCJ, Shi R, Yang C, Gao J, Zhou C, Li Q *et al.* 2019. Hierarchical transcription-factor and chromatin binding network for wood formation in *Populus trichocarpa*. *Plant Cell* **31**: 602–626.

Felten J, Vahala J, Love J, Gorzsás A, Rüggeberg M, Delhomme N, Leśniewska J, Kangasjärvi J, Hvidsten TR, Mellerowicz EJ *et al.* 2018. Ethylene signaling induces gelatinous layers with typical features of tension wood in hybrid aspen. *New Phytologist* **218**: 999–1014.

Fengel D, Wegener G. 2003. *Wood—Chemistry, ultrastructure, reactions.* Remagen, Germany: Kessel.

Gerber L, Eliasson M, Trygg J, Moritz T, Sundberg B. 2012. Multivariate curve resolution provides a high-throughput data processing pipeline for pyrolysis-gas chromatography/mass spectrometry. *Journal of Analytical and Applied Pyrolysis* **95**: 95–100.

Goodstein DM, Shu S, Howson R, Neupane R, Hayes RD, Fazo J, Mitros T, Dirks W, Hellsten U, Putham N *et al.* 2012. Phytozome: a comparative platform for green plant genomics. *Nucleic Acids Research* **40**: 1178–1186.

Gorshkova T, Mokshina N, Chernova T, Ibragimova N, Salnikov V, Mikshina P, Tryfona T, Banasiak A, Immerzeel P, Dupree P *et al.* 2015. Aspen tension wood fibers contain β-(1—> 4)-galactans and acidic arabinogalactans retained by cellulose microfibrils in gelatinous walls. *Plant Physiology* **169**: 2048–2063.

Hernández-Blanco C, Feng DX, Hu J, Sánchez-Vallet A, Deslandes L, Llorente F, Berrocal-Lobo M, Keller H, Barlet X, Sánchez-Rodríguez C *et al.* 2007. Impairment of cellulose synthases required for *Arabidopsis* secondary cell wall formation enhances disease resistance. *Plant Cell* **19**: 890–903.

Hiratsu K, Matsui K, Koyama T, Ohme-Takagi M. 2003. Dominant repression of target genes by chimeric repressors that include the EAR motif, a repression domain, in *Arabidopsis*. *The Plant Journal* **34**: 733–739.

Janz D, Lautner S, Wildhagen H, Behnke K, Schnitzler JP, Rennenberg H, Fromm J, Polle A. 2012. Salt stress induces the formation of a novel type of "pressure wood" in two *Populus* species. *New Phytologist* **194**: 129–141.

Karimi M, Inzé D, Depicker A. 2002. GATEWAY vectors for *Agrobacterium*-mediated plant transformation. *Trends in Plant Science* **7**: 193–195.

Kubo M, Udagawa M, Nishikubo N, Horiguchi G, Yamaguchi M, Ito J, Mimura T, Fukuda H, Demura T. 2005. Transcription switches for

© 2019 The Authors
New Phytologist © 2019 New Phytologist Trust

protoxylem and metaxylem vessel formation. *Genes & Development* **19**: 1855–1860.

Kudo M, Kidokoro S, Yoshida T, Mizoi J, Todaka D, Fernie AR, Shinozaki K, Yamaguchi-Shinozaki K. 2017. Double overexpression of DREB and PIF transcription factors improves drought stress tolerance and cell elongation in transgenic plants. *Plant Biotechnology Journal* **15**: 458–471.

Kumar M, Campbell L, Turner S. 2016. Secondary cell walls: biosynthesis and manipulation. *Journal of Experimental Botany* **67**: 515–531.

Lee DK, Jung H, Jang G, Jeong JS, Kim YS, Ha SH, Do Choi Y, Kim JK. 2016. Overexpression of the OsERF71 Transcription Factor Alters Rice Root Structure and Drought Resistance. *Plant Physiology* **172**: 575–588.

Legland D, Arganda-Carreras I, Andrey P. 2016. MorphoLibJ: integrated library and plugins for mathematical morphology with ImageJ. *Bioinformatics* **32**: 3532–3534.

Lin JS, Huang XX, Li Q, Cao Y, Bao Y, Meng XF, Li YJ, Fu C, Hou BK. 2016. UDP-glycosyltransferase 72B1 catalyzes the glucose conjugation of monolignols and is essential for the normal cell wall lignification in *Arabidopsis thaliana*. *The Plant Journal* **88**: 26–42.

Liu Y, Wei M, Hou C, Lu T, Liu L, Wei H, Cheng Y, Wei Z. 2017. Functional characterization of *Populus* PsnSHN2 in coordinated regulation of secondary wall components in tobacco. *Scientific Reports* **7**: 42.

Love J, Björklund S, Vahala J, Hertzberg M, Kangasjärvi J, Sundberg B. 2009. Ethylene is an endogenous stimulator of cell division in the cambial meristem of *Populus*. *Proceedings of the National Academy of Sciences, USA* **106**: 5984–5989.

Love MI, Huber W, Anders S. 2014. Moderated estimation of fold change and dispersion for RNA-seq data with DESeq2. *Genome Biology* **15**: 550.

Lucas WJ, Groover A, Lichtenberger R, Furuta K, Yadav SR, Helariutta Y, He XQ, Fukuda H, Kang J, Brady SM *et al.* 2013. The plant vascular system: evolution, development and functions. *Journal of Integrative Plant Biology* **55**: 294–388.

Ma R, Xiao Y, Lv Z, Tan H, Chen R, Li Q, Chen J, Wang Y, Yin J, Zhang L *et al.* 2017. AP2/ERF transcription factor, Ii049, positively regulates lignan biosynthesis in *Isatis indigotica* through activating salicylic scid Signaling and lignan/lignin pathway genes. *Frontiers in Plant Science* **8**: 1361.

McLeay RC, Bailey TL. 2010. Motif Enrichment Analysis: a unified framework and an evaluation on ChIP data. *BMC Bioinformatics* **11**: 165.

Muñiz L, Minguet EG, Singh SK, Pesquet E, Vera-Sirera F, Moreau-Courtois CL, Carbonell J, Blázquez MA, Tuominen H. 2008. ACAULIS5 controls *Arabidopsis* xylem specification through the prevention of premature cell death. *Development* **135**: 2573–2582.

Nilsson O, Aldén T, Sitbon F, Little CHA, Chalupa V, Sandberg G, Olsson O. 1992. Spatial pattern of cauliflower mosaic virus 35S promoter-luciferase expression in transgenic hybrid aspen trees monitored by enzymatic assay and non-destructive imaging. *Transgenic Research* **1**: 209–220.

Ohashi-Ito K, Iwamoto K, Fukuda H. 2018. LOB DOMAIN-CONTAINING PROTEIN 15 positively regulates expression of *VND7*, a master regulator of tracheary elements. *Plant and Cell Physiology* **59**: 989–996.

Ohtani M, Akiyoshi N, Takenaka Y, Sano R, Demura T. 2017. Evolution of plant conducting cells: perspectives from key regulators of vascular cell differentiation. *Journal of Experimental Botany* **68**: 17–26.

Pitre FE, Lafarguette F, Boyle B, Pavy N, Caron S, Dallaire N, Poulin PL, Ouellet M, Morency MJ, Wiebe N *et al.* 2010. High nitrogen fertilization and stem leaning have overlapping effects on wood formation in poplar but invoke largely distinct molecular pathways. *Tree Physiology* **30**: 1273–1289.

Pound MP, French AP, Wells DM, Bennett MJ, Pridmore TP. 2012. CellSeT: novel software to extract and analyze structured networks of plant cells from confocal images. *Plant Cell* **24**: 1353–1361.

Sato T. 1968. A modified method for lead staining of thin sections. *Journal of Electron Microscopy* **17**: 158–159.

Schurch NJ, Schofield P, Gierliński M, Cole C, Sherstnev A, Singh V, Wrobel N, Gharbi K, Simpson GG, Owen-Hughes T *et al.* 2016. How many biological replicates are needed in an RNA-seq experiment and which differential expression tool should you use? *RNA* **22**: 839–851.

Seyfferth C, Wessels B, Jokipii-Lukkari S, Sundberg B, Delhomme N, Felten J, Tuominen H. 2018. Ethylene-related gene expression networks in wood formation. *Frontiers in Plant Science* **9**: 272.

Sluiter A, Hames B, Ruiz R, Scarlata C, Sluiter J, Templeton D, Crocke D. 2008. Determination of structural carbohydrates and lignin in biomass. Laboratory Analytical Procedure (LAP). Technical Report National Renewable Energy Laboratory NREL/TP-510-42618. Denver, Colorado: National Renewable Energy Laboratory.

Smet W, De Rybel B. 2016. Genetic and hormonal control of vascular tissue proliferation. *Current Opinion in Plant Biology* **29**: 50–56.

Spurr AR. 1969. A low-viscosity epoxy resin embedding medium for electron microscopy. *Journal of Ultrastructure Research* **26**: 31–43.

Sun S, Yu JP, Chen F, Zhao TJ, Fang XH, Li YQ, Sui SF. 2008. TINY, a Dehydration-Responsive Element (DRE)-binding protein-like transcription factor connecting the DRE- and ethylene-responsive element-mediated signaling pathways in *Arabidopsis*. *Journal of Biological Chemistry* **283**: 6261–6271.

Sundell D, Mannapperuma C, Netotea S, Delhomme N, Lin YC, Sjödin A, Van de Peer Y, Jansson S, Hvidsten TR, Street NR. 2015. The plant genome integrative explorer resource: PlantGenIE.org. *New Phytologist* **208**: 1149–1156.

Sundell D, Street NR, Kumar M, Mellerowicz EJ, Kucukoglu M, Johnsson C, Kumar V, Mannapperuma C, Delhomme N, Nilsson O *et al.* 2017. AspWood: high-spatial-resolution transcriptome profiles reveal uncharacterized modularity of wood formation in *Populus tremula*. *Plant Cell* **29**: 1585–1604.

Sweeley CC, Bentley R, Makita M, Wells WW. 1963. Gas-liquid chromatography of trimethylsilyl derivatives of sugars and related substances. *Journal of the American Chemical Society* **85**: 2497–2507.

Taylor-Teeples M, Lin L, de Lucas M, Turco G, Toal TW, Gaudinier A, Young NF, Trabucco GM, Veling MT, Lamothe R *et al.* 2015. An *Arabidopsis* gene regulatory network for secondary cell wall synthesis. *Nature* **517**: 571–575.

Trygg J, Wold S. 2002. Orthogonal projections to latent structures (O-PLS). *Journal of Chemometrics* **16**: 119–128.

Vahala J, Felten J, Love J, Gorzsás A, Gerber L, Lamminmäki A, Kangasjärvi J, Sundberg B. 2013. A genome-wide screen for ethylene-induced ethylene response factors (ERFs) in hybrid aspen stem identifies ERF genes that modify stem growth and wood properties. *New Phytologist* **200**: 511–522.

Wang Y, Chen Y, Ding L, Zhang J, Wei J, Wang H. 2016. Validation of reference genes for gene expression by Quantitative Real-Time RT-PCR in stem segments spanning primary to secondary growth in *Populus tomentosa*. *PLoS ONE* **11**: e0157370.

Xue LJ, Frost CJ, Tsai CJ, Harding SA. 2016. Drought response transcriptomes are altered in poplar with reduced tonoplast sucrose transporter expression. *Scientific Reports* **6**: 33655.

Yu L, Ma J, Niu Z, Bai X, Lei W, Shao X, Chen N, Zhou F, Wan D. 2017. Tissue-specific transcriptome analysis reveals multiple responses to salt stress in *Populus euphratica* seedlings. *Genes* **8**: E372.

Zeng JK, Li X, Xu Q, Chen JY, Yin XR, Ferguson IB, Chen KS. 2015. EjAP2-1, an AP2/ERF gene, is a novel regulator of fruit lignification induced by chilling injury, via interaction with EjMYB transcription factors. *Plant Biotechnology Journal* **13**: 1325–1334.

Zhang G, Chen M, Li L, Xu Z, Chen X, Guo J, Ma Y. 2009. Overexpression of the soybean GmERF3 gene, an AP2/ERF type transcription factor for increased tolerances to salt, drought, and diseases in transgenic tobacco. *Journal of Experimental Botany* **60**: 3781–3796.

Zhao C, Avci U, Grant EH, Haigler CH, Beers EP. 2008. XND1, a member of the NAC domain family in *Arabidopsis thaliana*, negatively regulates lignocellulose synthesis and programmed cell death in xylem. *The Plant Journal* **53**: 425–436.

Zhong R, McCarthy RL, Lee C, Ye ZH. 2011. Dissection of the transcriptional program regulating secondary wall biosynthesis during wood formation in poplar. *Plant Physiology* **157**: 1452–1468.

Zhong R, Richardson EA, Ye ZH. 2007. Two NAC domain transcription factors, SND1 and NST1, function redundantly in regulation of secondary wall synthesis in fibers of *Arabidopsis*. *Planta* **225**: 1603–1611.

Zhou ML, Ma JT, Zhao YM, Wei YH, Tang YX, Wu YM. 2012. Improvement of drought and salt tolerance in *Arabidopsis* and *Lotus corniculatus* by overexpression of a novel DREB transcription factor from *Populus euphratica*. *Gene* **506**: 10–17.

© 2019 The Authors
New Phytologist © 2019 New Phytologist Trust

Zhou J, Zhong R, Ye ZH. 2014. *Arabidopsis* NAC Domain Proteins, VND1 to VND5, are transcriptional regulators of secondary wall biosynthesis in vessels. *PLoS ONE* **9**: e105726.

Supporting Information

Additional Supporting Information may be found online in the Supporting Information section at the end of the article.

Fig. S1 Transgene expression in the transgenic ERF139-SRDX lines.

Fig. S2 FT-IR analysis in normal wood of ERF139OE and ERF139-SRDX trees compared with the WT.

Fig. S3 Characterization of wood anatomy in ERF139OE trees.

Fig. S4 Identification of primary targets of ERF139 by transcriptome analysis of ERF139OE and ERF139-SRDX trees.

Fig. S5 *ERF139* expression marks the zone of transcriptional initiation of SCW formation.

Table S1 Raw data and summary of the pyrolysis GC-MS data.

Table S2 DEGs identified in ERF139OE vs WT.

Table S3 DEGs identified in ERF139-SRDX vs WT.

Table S4 Functional categorization of DEGs in ERF139OE and ERF139-SRDX.

Table S5 Primary targets of ERF139.

Table S6 Expression of genes related to lignin biosynthesis and polymerization in ERF139OE and ERF139-SRDX.

Table S7 Primers used in this study.

Please note: Wiley Blackwell are not responsible for the content or functionality of any Supporting Information supplied by the authors. Any queries (other than missing material) should be directed to the *New Phytologist* Central Office.

About *New Phytologist*

- *New Phytologist* is an electronic (online-only) journal owned by the New Phytologist Trust, a **not-for-profit organization** dedicated to the promotion of plant science, facilitating projects from symposia to free access for our Tansley reviews and Tansley insights.
- Regular papers, Letters, Research reviews, Rapid reports and both Modelling/Theory and Methods papers are encouraged. We are committed to rapid processing, from online submission through to publication 'as ready' via *Early View* – our average time to decision is <26 days. There are **no page or colour charges** and a PDF version will be provided for each article.
- The journal is available online at Wiley Online Library. Visit **www.newphytologist.com** to search the articles and register for table of contents email alerts.
- If you have any questions, do get in touch with Central Office (np-centraloffice@lancaster.ac.uk) or, if it is more convenient, our USA Office (np-usaoffice@lancaster.ac.uk)
- For submission instructions, subscription and all the latest information visit **www.newphytologist.com**

© 2019 The Authors
New Phytologist © 2019 New Phytologist Trust